Properties of BSi_6N monolayers derived by first-principle computation

Nzar Rauf Abdullah[a,b], Hunar Omar Rashid[a], Chi-Shung Tang[c], Andrei Manolescu[d], Vidar Gudmundsson[e]

[a] *Division of Computational Nanoscience, Physics Department, College of Science, University of Sulaimani, Sulaimani 46001, Kurdistan Region, Iraq*
[b] *Computer Engineering Department, College of Engineering, Komar University of Science and Technology, Sulaimani 46001, Kurdistan Region, Iraq*
[c] *Department of Mechanical Engineering, National United University, 1, Lienda, Miaoli 36003, Taiwan*
[d] *Reykjavik University, School of Science and Engineering, Menntavegur 1, IS-101 Reykjavik, Iceland*
[e] *Science Institute, University of Iceland, Dunhaga 3, IS-107 Reykjavik, Iceland*

arXiv:2008.03782v1 [cond-mat.mtrl-sci] 9 Aug 2020

Abstract

The buckling effects due to BN-bonds in BN-codoped silicene, BSi_6N, on structural stability, electronic band structure, and mechanical, thermal and optical properties are studied systematically by first-principle calculations within density functional theory. In the presence of BN-bonds, a high warping in BSi_6N indicating a high buckling effect is found due to the presence of a repulsive interaction between B and N atoms. It thus breaks the sublattice symmetry of silicene and opens up a bandgap. The high buckling of BSi_6N leads to a decrease in its stiffness and thus induces fractures at small values of applied strain. The finite bandgap caused by the BN-bonds leads to enhancement of the Seebeck coefficient and the figure of merit, and induces a redshift of a peak in the dielectric response. By increasing the distance between the B and N atoms i.e. for the BSi_6N without BN-bonds, a flatter BSi_6N is found compared to pristine silicene. The stiffness of the structure and the ultimate strain are increased. The breaking of the sublattice symmetry is very weak and a very small bandgap is revealed. As a result, the Seebeck coefficient and the figure of merit stay very small. A reduction in the optical response is seen due to an indirect bandgap.

Keywords: Energy harvesting, Thermal transport, Silicene, Density Functional Theory, Electronic structure, Optical properties, and Stress-strain curve

1. Introduction

Two-dimensional (2D) materials are at the heart of nanotechnology because of their outstanding physical and chemical properties, and their potential applications in nanoelectronics [1, 2]. Silicon structures indicating graphene-like silicene, a 2D material system exhibiting semi-metal properties caused by a zero bandgap, were experimentally investigated by Aufrey et al. [3]. The first theoretical study of silicene was in 1994 using first-principles total-energy calculations [4]. Afterwards, the electrical, thermal and optical properties of silicene have been extensivly investigated for understanding the structure. In fact, the zero bandgap limits the application of silicene in nanoelectronics despite of its high carrier mobility [5]. Therefore, several techniques have been used to tune the bandgap to enhance the functionality of silicene in technologies [6], such as using an external electric field oriented perpendicular to the monolayer of Si atoms [7], bond symmetry breaking with uniaxial strain [8], surface adsorption [9], alkali metal intercalation [10], and substitutional doping of Boron- and Nitrogen-codoped silicene [11].

It has been found that silicene is relatively weaker than other 2D materials such as graphene in terms of stiffness and strength. In addition, it is more rigid when subject to bending, due to its slightly buckled molecular geometry [12]. Silicene exhibits a strain-induced self-doping phenomenon, which is also closely related to its buckled structure, that cannot arise in graphene [13]. Therefore, its mechanical properties are different compared to other 2D planar materials. It has been shown that a silicene lattice is stable up to 17% under biaxial tensile strain [14]. Qin et al. proposed that the in-plane stiffness of silicene is much weaker than that of graphene. So, the obtained strain is close to 20% under uniform expansion in ideal conditions [15]. The nonlinear elasticity of silicene has been investigated and it has been demonstrated that the deformation and failure behavior, and the ultimate strength are all anisotropic [16].

Thermoelectric energy conversion in 2D materials such as silicene [17] with impurities [18, 19] has attracted tremendous interest due to significant potential for industrial applications. Theoretical studies of the electron and the phonon thermal conductivity have been reported [20, 21]. Using equilibrium molecular dynamic simulations and the Kubo-Green method together, the thermal conductivity of silicene has been predicted to be

Email address: nzar.r.abdullah@gmail.com (Nzar Rauf Abdullah)

20 W $m^{-1}K^{-1}$. In non-equilibrium molecular dynamics simulations, the thermal conductivity of a monolayer silicene under uniaxial stretching is found to be around 40 $Wm^{-1}K^{-1}$ [22]. The Boltzmann Transport Equation has also been utilized to investigate the thermal properties of silicene and it indicated a conductivity about 9.4 $Wm^{-1}K^{-1}$ at 300 K. In all cases the thermal conductivity is much lower than for bulk silicon [23]. Furthermore, the Seebeck coefficient and the figure of merit have been reported using first-principle density functional techniques and linear response in which the higher figure of merit for distorted silicene is demonstrated [24], and for silicene nanoribbons it can be up to 160 [25]. Recently, Boltzmann theory for electrons under the relaxation time approximation has been employed to obtain the Seebeck coefficient showing that hydrogenation can greatly improve the electronic figure of merit, ZT_e, of multilayer silicene [26].

Another interesting aspect of silicene is its role in optical applications such as in the optoelectronic industry, in photo-detectors, sensors, low power lasers and not least in fiber optics communication [27, 28]. Optical response characteristics indicate that they strongly depend on the direction of polarization of the light [29]. The dielectric functions, and optical absorption are hence different for light polarized parallel, $E_{\parallel}$, and perpendicular, $E_{\perp}$, to the plane of silicence [30]. The optical response may also be changed by tuning the bandgap via a geometrical modification of a silicene nanosheet such as its width. As a result, a broad frequency photoresponse ranging from far infrared to ultraviolet is found [31]. At low-frequency regime under an in-plane polarized driving field, the dynamical polarization, the dielectric function, and an absorption of a radiation in the infrared region have been obtained [32].

In this paper, we study the electronic, mechanical, optical, and thermal properties of silicene chemically modified by various Boron (B), and Nitrogen (N) atoms configurations doped in the silicene nanosheet structure, BSi_6N. In addition, the stability and formation energy calculated via density functional theory (DFT) are demonstrated. We show how different BN isomers that form BN-bonds influence the shape of BSi_6N via a buckling degree. Tuning the buckling degree caused by the BN-bonds influences the entire physical properties of the system as will be discussed in the Results section.

In Sec. 2 the silicene structure is briefly over viewed. In Sec. 3 the main achieved results are analyzed. In Sec. 4 the conclusion of the results is presented.

2. Computational Tools

Crystalline and molecular structure visualization programs (XCrySDen) and VESTA are employed to visualize all the structures presented in this work [33, 34]. After modeling the pristine silicene and BSi_6N structures, we use density functional theory employing the generalized gradient approximation (GGA) with the Perdew-Burke-Ernzerhof (PBE) functionals [35]. The DFT calculations based on the standard KohnSham (KS) equations are performed using the Quantum Espresso (QE) package [36, 37]. The Brillouin-Zone (BZ) sampling integrations have been achieved using sets of points corresponding to a $14 \times 14 \times 1$ Monkhorst-Pack mesh [38]. The convergence of the mesh cut-off is checked and we find that at the value of 1088.45 eV the GGA the model is converged with respect to our results. A geometry optimization is obtained with all residual forces being less than 10^{-6} eV/Å. The distance between periodically repeated images of the different systems along the z-direction is set to at least 20 Å. In the density of state (DOS) calculations, a $77 \times 77 \times 1$ grid points mesh is used.

Bader charge analysis has been done using the Henkelman code for analysing the transfer rate of charge between atoms [39]. In addition, a Boltzmann transport theory (BoltzTraP) is used to study thermal properties of the systems [40]. The BoltzTraP code employs a mesh of band energies and is interfaced to the QE package [41]. The optical properties of the systems are evaluated by the QE code. An optical broadening of 0.1 eV is assumed for the calculation of the dielectric properties.

3. Results

In this section, we present our model, the calculation of the formation energy, the electronic properties including the band structure, the mechanical, the thermal, and the optical properties of pristine silicene and the BSi_6N structure. We assume a 2×2 supercell of buckled silicene structure presented in Fig. 1(a). The buckled nature of silicene is caused by the positions of the Si atoms in the A and B sites that do not lie in the same plane leading to a staggered sublattice potential and a layer separation between the two sublattices of A and B sites. In addition to pure buckled silicene (b-Si), three BN-codoped silicene structures (three isomers) are considered where the B atom (blue) is fixed at a para position at the top of the hexagon [42]. In isomer b, the B and N (red) are at the ortho positions lead to BN-bonds, in isomer c same type of dopants (B or N) are placed at the adjacent positions, in isomer d, B and N are at the para positions [43]. The isomer b, c, and d are identified as BSi_6N-1, BSi_6N-2, BSi_6N-3, respectively. The numbers of 1, 2, and 3 are linked to BSi_6N for distinguishing these three structures. After fully relaxation of b-Si, the hexagonal lattice constant, a, the buckling length, δ, and the Si-Si bond length of pristine b-Si are 3.86 Å, 0.446 Å, 2.26 Å, respectively, (see Tab. 1). These values are in a good agreement with previous studies of slightly buckled silicenes [44]. The lattice constants, the buckling lengths, and the bond lengths of BSi_6N structures are also listed in Tab. 1.

We can see from Tab. 1 that the B and N atoms configurations influence the lattice constant, and the buckling lengths. The bond lengths in turn affect the sublattice

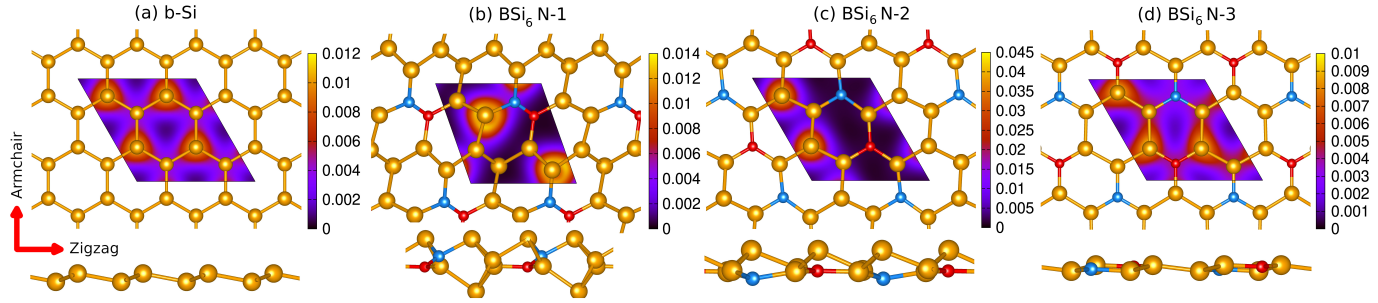


Figure 1: Pristine buckled silicene (b-Si) (a), BN-codoped silicene identified as BSi_6N-1 (b), BSi_6N-2 (c), and BSi_6N-3 (d). The Si, B and N atoms are golden, blue and red colored, and the bottom panel is the side view of the corresponding structures. The contour plot is the electron charge distribution in a 2×2 supercell.

Table 1: Lattice constant, a, buckling length, δ, Si-Si, B-N, Si-B, and Si-N bonds for all b-Si and BN-codoped structures. The unit of all parameters is Å.

Structure	a	δ	Si-Si	B-N	Si-B	Si-N
b-Si	3.86	0.446	2.26	-	-	-
BSi_6N-1	3.41	1.301	2.38	1.377	2.064	1.779
BSi_6N-2	3.37	0.682	2.22	-	1.92	1.831
BSi_6N-3	3.42	0.281	2.25	-	1.87	1.81

symmetry of the system and the bandgap. In presence of BN-bonds, in BSi_6N-1, the buckling degree is strongly affected and the structure records the highest buckling length, $d = 1.301$ Å. As a result, the structure is strongly warped as is shown in the side view (bottom panel) of Fig. 1(b).

If the B and N atoms are doped in silicene in such a way that one Si atom is located between these two atoms (see Fig. 1(c)), the buckling length of BSi_6N-2 gets smaller, $d = 0.682$ Å, or the distortion becomes smaller comparing to BSi_6N-1. Increasing further the distance between the B and N atoms, see Fig. 1(d), the structure is close to the pristine b-Si structure or even flatter as $d = 0.281$ Å. The warping and flattening of these structures are attributed to the interaction between the B and N atoms. This issue will be discussed later.

The contour plots in Fig. 1 represent the electron charge distributions in which the charge density of those atoms near to the surface is high. The charge distribution of BSi_6N-1 indicates that the electron densities are not delocalized along the B-N bond. This suggests a repulsive interaction between B and N atoms [45]. On the other hand, a Bader charge analysis demonstrates that an N atoms in BSi_6N-3 gain more charge from the surrounding Si atoms as the repulsive interaction between the B and N atoms does not play an important role there. Therefore, a charge accumulation around the N atoms is observed.

3.1. Structural stability

The isomers in which the BN-bonds are present (ortho positions), have considerably larger cohesive energy and are hence more stable than their counterparts (para positions) in which the B and the N atoms are apart. This is due to the more stability of the BN bond than the BSi or the NSi bonds. On the other hand, the formation energy can be used to find the most stable structure. The formation energy, E_f, of a doped system is defined in terms of the structural energy of a cell containing N_i atoms of species i,

$$E_f = E_T - N_{Si}\,\mu_{Si} - N_B\,\mu_B - N_N\,\mu_N \qquad (1)$$

where E_T is the total energy of the BN-codoped silicene structure, N_{Si}, N_B, and N_N are the number of Si, B and N atoms, respectively, and μ_{Si}, μ_B, and μ_N, are the chemical potential of the Si, B and N atoms, respectively. The chemical potential is determined by the energy per atom. Using Eq. (1) the formation energy of BSi_6N-1, BSi_6N-2, BSi_6N-3 are -122.16, -120.59 and -121.05 eV, respectively, indicating that the BSi_6N-1 is energetically the most stable structure among these three structures.

3.2. Interaction energy

The interaction energy between the B and N atoms doped in the silicene structure can be calculated from the total energy. In BN-codoped graphene, the interaction between the B and the N atoms indicates that B-B and N-N interactions in the system are repulsive whereas the NB interaction is attractive [45]. In our BN-codoped silicene, the Bader charge analysis indicates the repulsive interaction between B and N atoms as both doped atoms are positively charged. In addition, the interaction energy in BN-codoped graphene is inversely varied with the distance between B and N atoms, and the interaction strength is almost zero when the separation distance is greater than or equal to 4.0 Å [46]. So, we expect that the interaction between B and N atoms in silicene is also inversely proportional to the distance between these two atoms.

After fully relaxing our systems, we found that the distance between the B and N atoms in BSi_6N-1, BSi_6N-2, and BSi_6N-3 is 1.377, 3.428, and 4.085 Å, respectively. Furthermore, the total energy obtained from the SCF calculations indicates that the interaction between B and N atoms in BSi_6N-1 is maximum while in BSi_6N-3 is almost

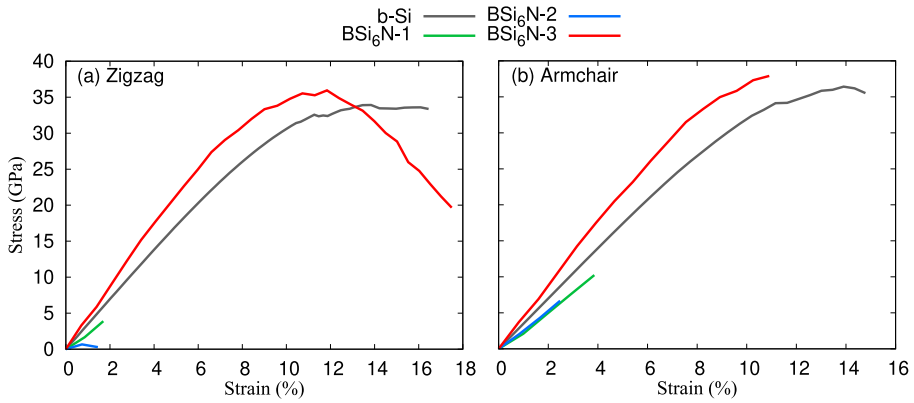


Figure 2: Stress-strain curves of pure b-Si (gray), BSi_6N-1 (green), BSi_6N-2 (blue), and BSi_6N-3 (red) for zigzag (a) and armchair (b) directions. The systems are subjected to uniaxial strain.

zero [47]. This is the reason that the BSi_6N-1 and BSi_6N-3 are the most warped and flattened structures, respectively.

3.3. Mechanical properties

The DFT calculations can be utilized to study the mechanical properties of single-layer and freestanding silicene. Uniaxial tensile simulations are carried out to probe the stress-strain properties. This can be obtained by gradually applying load in the zigzag or armchair directions of a structure [48]. During uniaxial tensile loading, the periodic dimension along the loading direction is increased step-by-step with a fixed strain of 0.02.

The stress-strain curves for three BSi_6N structures are plotted together with the one for the b-Si in Fig. 2 for the x-, the zigzag, (a) and the y-, the armchair direction (b). We first focus on the pure b-Si structure (gray). The first observation is that the buckling length of the sheets gradually decreases by increasing strain level. A linear relation between the stress and strain reflecting an increase in the in-plane stiffness and elastic property is seen. The linear elastic regime for the pure b-Si ends at $\approx 10\%$ (gray) in both zigzag and armchair directions revealing isotropic elastic response. Higher strain leads to a stretching of the Si-Si bonds and, therefore, a decrease in the in-plane stiffness. The ultimate strength of pure b-Si structure in the zigzag direction is 33.92 GPa at strain 13.8% while in the armchair direction it is 36.42 GPa at strain 13.9%. As we have mentioned before, silicene is relatively weak structure comparing to other 2D materials such as graphene due to its buckled geometry. We therefore expect that the ultimate strength of silicene is lower than that of graphene [49, 45, 50].

In the BSi_6N structures, the interaction between B and N atoms and BN-bonds play an essential role on stress-strain curve. Both BSi_6N-1 (green), and BSi_6N-2 (blue) induce fracture strain very early at strain less than 1.7% in the zigzag direction and 4% in the armchair direction. The small BN-bond length and the larger Si-Si bond in BSi_6N-1 comparing to b-Si, and the relatively strong repulsive interaction between the B and N atoms in BSi_6N-1 induces a strong deformation and larger buckling length. A higher buckling length, and a less in-plane stiffness is obtained. Therefore, the fracture strain of both BSi_6N-1 and BSi_6N-2 is small.

The stress-strain curve of the last structure, BSi_6N-3 (red), is interesting and completely different from BSi_6N-1 and BSi_6N-2 because the repulsive interaction between B and N atoms is almost zero. The elastic region here is decreased to $\approx 6.5\%$ in the zigzag and $\approx 7.5\%$ in the armchair directions indicating anisotropic mechanical properties of the structure in the elastic region. The ultimate strength is 35.94 GPa at strain 11.84% and 37.9 GPa at strain 10.9%, in the zigzag and armchair directions, respectively. The ultimate strength of BSi_6N-3 in both direction is higher than that of pure b-Si. So BSi_6N-3 is mechanically the stronger structure.

3.4. Electronic properties

In this section, we discuss the electronic band structure of pure silicene and BSi_6N using DFT. In Fig. 3, we plot the band structure of b-Si (a), BSi_6N-1 (b), BSi_6N-2 (c), and BSi_6N-3 (d) along the high symmetry points in the Brillouin zone. The linear dispersion of b-Si band structure around the Fermi level indicates the semimetallic nature where valence band maxima (π band) and the conduction band minima (π^* band) touch each other only at the high symmetry K point. The linear dispersion in pure b-Si shows that the charge carriers around the Fermi level will act like massless Dirac-Fermions. The Hamiltonian that introduces the electronic structure of b-Si around the Dirac point can be written as [45]

$$\hat{H} = \begin{pmatrix} \Delta & \hbar v_F(k_x - ik_y) \\ \hbar v_F(k_x + ik_y) & \Delta \end{pmatrix} \qquad (2)$$

Herein, Δ, v_F, and k refer to onsite energy difference between the Si atoms located at A and B sites, Fermi velocity, and momentum of charge carriers. The linear relation refers to the zero value of the onsite energy difference, Δ, in b-Si arising from the presence of inversion symmetry in b-Si.

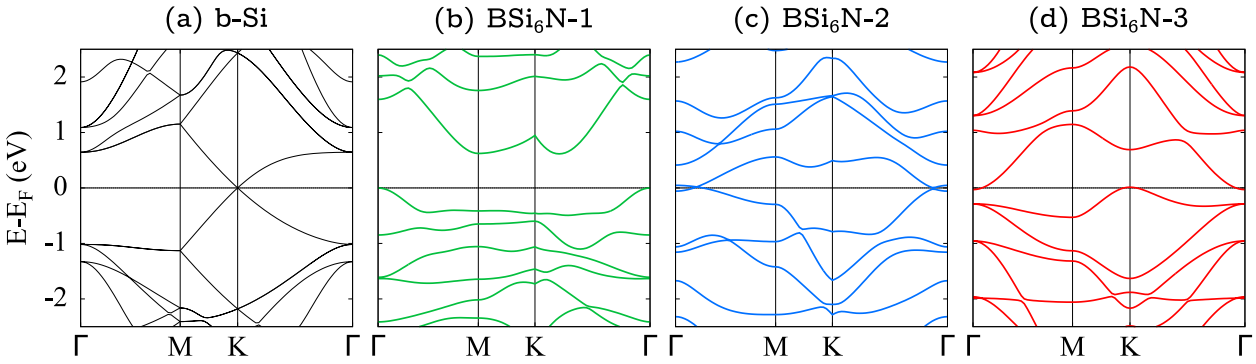


Figure 3: Band structure for optimized structures of b-Si (a), BSi_6N-1 (b), BSi_6N-2 (c), and BSi_6N-3 (d). The energies are with respect to the Fermi level, and the Fermi energy is set to zero.

In BSi_6N structures, the band structure is importantly modified as a bandgap is opened and tuned depending on the B and N atoms configurations as is shown in Fig. 3(b-d). In general, a band gap in BSi_6N is opened near the K point due to breaking of the inversion symmetry by the distortion generated by the B and N atoms configuration. The reason for the broken symmetry is that the potential seen by the atoms at sites A and B is now different, leading to a finite value of onsite energy $\Delta \neq 0$, where $\Delta = \alpha(V_A - V_B)$ with α being a constant value and $V_A(V_B)$ is the potential seen by an atom at the site A(B). On the other hand, the potential difference is directly proportional to the buckling parameter, $V_A - V_B \sim \delta$, where δ is the buckling parameter [51].

In BSi_6N-1 (b), the buckling parameter, δ, has the highest value among three BN-codoped structures leading to an opening of a bandgap and the linear dispersion at K point is not seen anymore. The BSi_6N-2 (c) has an intermediate buckling length and the opening bandgap at the K point is still observed but the Fermi energy slightly crosses the valence band maxima near the Γ point leading to degenerate semiconductor behavior of BSi_6N-2. This is very much consistent with study of N-doped silicene reported in [52]. In the last structure, BSi_6N-3 (d), the buckling parameter is low but the potential difference between A and B sites leads to an indirect bandgap along the K and the Γ points.

3.5. Thermal properties

The study of thermal properties of pure silicene and BSi_6N sheets is important for thermoelectric energy conversion which is the ability of a device to convert temperature gradient into an electrical current. The figure of merit, ZT, reflecting the efficiency of a device and the Seebeck coefficient, S, are calculated here. The figure of merit is defined as $ZT = \sigma S^2 T/\kappa$, where σ is the electric conductance, T is the absolute temperature, and $\kappa = \kappa_e + \kappa_p$ is the total thermal conductance that consists of the electron, κ_e and the phonon, κ_p contributions. Silicene is thermally stable up to 1500 K which is attributed to a low phonon conductance. This is contrary to other 2D materials such as graphene, which exhibits a high thermal conductivity.

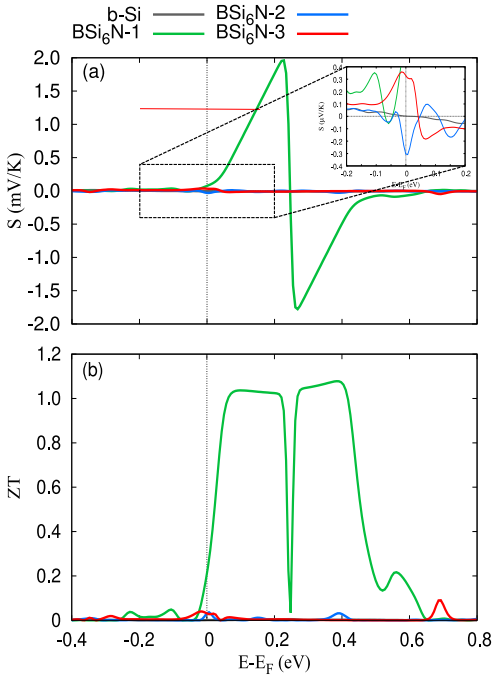


Figure 4: Seebeck coefficient (a), and the figure of merit (b) as a function of energy are plotted at $T = 100$ K for pristine b-Si (gray), BSi_6N-1 (green), BSi_6N-2 (blue), and BSi_6N-3 (red).

We show the thermal properties in the temperature range of T = 20-160 K where the electron and the lattice temperatures are decoupled and the energy exchange between the charge carriers and the acoustic phonons is very weak [53, 54, 55, 56]. As a result, only the electronic part of the thermal properties is dominant in this temperature range. To calculate the electronic thermal properties of a material, the BoltzTraP software is used.

The Seebeck coefficient (a) and the figure of merit (b) versus energy at $T = 100$ K are shown in Fig. 4 for pristine b-Si (gray), BSi_6N-1 (green), BSi_6N-2 (blue), and BSi_6N-3 (red). It can clearly be seen that both S and and ZT show large variations for BSi_6N-1. This is attributed to the presence of a larger bandgap in BSi_6N-1. The strong dip in ZT of BSi_6N-1 is expected as the S is zero at the same energy, 0.25 eV. The inset in Fig. 4a indicates S in

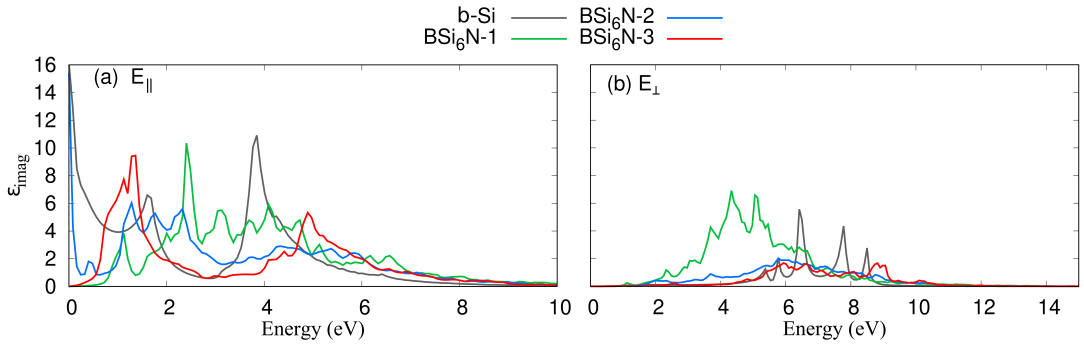


Figure 5: Imaginary part of dielectric function of pristine b-Si (gray), BSi_6N-1 (green), BSi_6N-2 (blue), and BSi_6N-3 (red) for parallel, $E_{\parallel}$, (a) and perpendicular, $E_{\perp}$, (b) polarized electric field.

the energy range of -2.0 to 2.0 eV. It is clear that the S for b-Si is smaller than BN-codoped silicene structures.

This is expected as the thermoelectric power in semiconductors of n and p types is approximately three orders of magnitude higher than that of metals. The change of sigh of the Seebeck coefficient indicates the transition between electron and hole dominated transport. In the n-type semiconductor, BSi_6N-1, there will be high thermoelectric figure of merit if there is a large energy difference between the conduction band minima and the Fermi energy, E_c-E_F, while for the p-type semiconductor E_F-E_v is important for similar behavior where E_v is the valence band maxima.

3.6. Optical properties

The optical properties of a material show how it interacts with electromagnetic field of an incident light [57, 58]. Optical characteristics are directly related to electronic band structure. So, tuning the bandgap of a material will influence its optical behavior.

To see the influences of B and N doping of silicene on its optical response, we present the imaginary part of the dielectric function, $\varepsilon_{\text{imag}}$, in Fig. 5 for light polarized parallel (a) and perpendicular (b) to the plane of the b-Si (gray), BSi_6N-1 (green), BSi_6N-2 (blue), and BSi_6N-3 (red). The imaginary part is related to the absorption of energy within the material. In order to obtain a more accurate optical response, we consider a finer large mesh size of k-points, $110 \times 110 \times 1$. It can be seen that the imaginary part of dielectric function changes with the direction of light polarization as the parallel and perpendicular components of $\varepsilon_{\text{imag}}$ are different. Another observation is that the $\varepsilon_{\text{imag}}$ in parallel polarized light is dominant below the energy range of 5 eV while in the case of perpendicular polarized of light $\varepsilon_{\text{imag}}$ is observed to be active above 5 eV. This anisotropy in $\varepsilon_{\text{imag}}$ has been reported and it is a consequence of the 2D nature of the buckled silicene sheet [59]. In pristine b-Si, two major peaks are found in energy range from 0 to 5.5 eV in the case of parallel polarized light. The first weaker peak is located at 1.68 eV indicating transition from π to π^* states which are close to the Fermi energy. The second peak is found at 3.85 eV corresponding to the σ to σ^* transitions. It should be mentioned that the shape of both peaks is almost symmetric which is related to the symmetry of π to π^* bands, and σ to σ^* bands. Similar to graphene, inter-band transitions for perpendicular polarized light, $E_{\perp}$, are observed for pristine b-Si except the transitions here occure below 10 eV (see Fig. 5(b) gray color).

In the BSi_6N structures, a redshift in the first peak corresponding to $\pi \rightarrow \pi^*$ transitions in the case of $E_{\parallel}$ is seen. The energy value of redshifted first peak is found to be 1.12, 1.28, and 1.36 eV for BSi_6N-1, BSi_6N-2, and BSi_6N-3, respectivily. The redshift can be referred to the opening of a bandgap along the M-K paths. In addition, the reduction in second peak for BSi_6N-1, and BSi_6N-2 in the case of $E_{\parallel}$ refers to the deformation and a further separation of the σ and σ^* bands arising from the warped BSi_6N-1, and BSi_6N-2 structures. But a blueshift and reduction in the second peak of BSi_6N-3 is seen which stands for the larger energy spacing between the σ and σ^* states. This is attributed to the smaller buckling parameter in BSi_6N-3. It has been reported that at a higher buckling degree a smaller energy spacing between σ and σ^* is obtained [60]. This is the reason why the energy spacing in band structure of planer silicene is higher than that of buckled silicene. The same senario can be applied to the main transition peaks for $E_{\perp}$.

The last study of our work is the electron energy loss function (EELF) which introduces the energy loss of a fast moving electron in a material. The EELF is shown in Fig. 6 for b-Si (gray), BSi_6N-1 (green), BSi_6N-2 (blue), and BSi_6N-3 (red) in the case of $E_{\parallel}$ (a) and $E_{\perp}$ (b). The peaks in ELLF indicate the point of transition from metallic to dielectric property of a material (the plasma frequency). In pristine b-Si, three peaks around 2.1, 5.9, and 7.95 eV are observed for $E_{\parallel}$, and the same peaks with a shift towards a higher energy are seen at 6.82, 8.17, and 9.06 eV for $E_{\perp}$. The first peak at 2.1 eV reveals a π plasmon, and the second peaks around 6 eV stand for a $\pi + \sigma$ plasmon. The presence of these peaks is due to collective excitations at different light energy. The peak position of b-Si in both directions of light polarization are in a good agreement

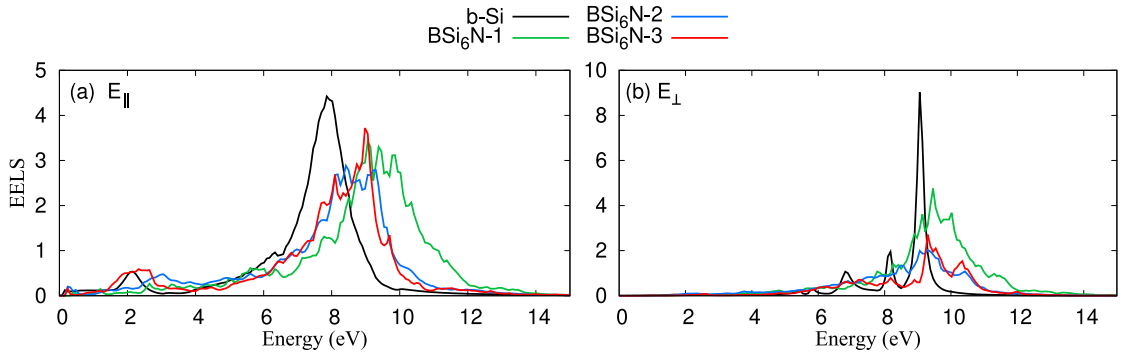


Figure 6: Electron energy loss spectroscopy (EELF) of pristine b-Si (gray), BSi_6N-1 (green), BSi_6N-2 (blue), and BSi_6N-3 (red) for parallel (a) and perpendicular (b) polarized electric field.

with previous studies of b-Si [61]. The peaks in the ELLF corresponds to the dip in the complex dielectric function in both directions of light polarization. We therefore see shifting in the ELLF peaks of all three BSi_6N structures.

4. Summary and Conclusions

Density functional theory was utilized for investigating the electronic characteristics of BSi_6N sheets, where the B and N atomic configuration and BN-bonds play a major role in opening bandgaps. It was shown that the repulsive interaction between the B and N atoms gives rise a high buckling degree in the system, which is reflected in a strongly broken sub-lattice symmetry of the system. The repulsive interaction between the B and N atoms is decreased by increasing distance between these two doped atoms. The high buckling degree in the presence of BN-bonds in BSi_6N reveals a weakness of the structure. As a result, the resistance to deformation in response to an applied strain is decreased. In addition, the opening of a bandgap in the presence of the BN-bonds increases the Seebeck coefficient and the figure of merit. This may be interesting in high thermoelectric efficiency nanodevices. A redshift towards low energy in the optical responses of BSi_6N has been found that may be interested in the regard of optoelectronic devices.

5. Acknowledgment

This work was financially supported by the University of Sulaimani and the Research center of Komar University of Science and Technology. The computations were performed on resources provided by the Division of Computational Nanoscience at the University of Sulaimani. CST acknowledges support from Ministry of Science and Technology in Taiwan, under grant No. MOST 109-2112-M-239-003.

References

[1] L. Tao, E. Cinquanta, D. Chiappe, C. Grazianetti, M. Fanciulli, M. Dubey, A. Molle, D. Akinwande, Silicene field-effect transistors operating at room temperature, Nature Nanotechnology 10 (3) (2015) 227–231. doi:10.1038/nnano.2014.325.
URL https://doi.org/10.1038/nnano.2014.325

[2] G. Le Lay, Silicene transistors, Nature Nanotechnology 10 (3) (2015) 202–203. doi:10.1038/nnano.2015.10.
URL https://doi.org/10.1038/nnano.2015.10

[3] B. Aufray, A. Kara, S. Vizzini, H. Oughaddou, C. Landri, B. Ealet, G. Le Lay, Graphene-like silicon nanoribbons on ag(110): A possible formation of silicene, Applied Physics Letters 96 (18) (2010) 183102. arXiv:https://doi.org/10.1063/1.3419932, doi:10.1063/1.3419932.
URL https://doi.org/10.1063/1.3419932

[4] K. Takeda, K. Shiraishi, Theoretical possibility of stage corrugation in si and ge analogs of graphite, Phys. Rev. B 50 (1994) 14916–14922. doi:10.1103/PhysRevB.50.14916.
URL https://link.aps.org/doi/10.1103/PhysRevB.50.14916

[5] F. Pan, Y. Wang, K. Jiang, Z. Ni, J. Ma, J. Zheng, R. Quhe, J. Shi, J. Yang, C. Chen, J. Lu, Silicene nanomesh, Scientific Reports 5 (1) (2015) 9075. doi:10.1038/srep09075.
URL https://doi.org/10.1038/srep09075

[6] J. Zhao, H. Liu, Z. Yu, R. Quhe, S. Zhou, Y. Wang, C. C. Liu, H. Zhong, N. Han, J. Lu, Y. Yao, K. Wu, Rise of silicene: A competitive 2d material, Progress in Materials Science 83 (2016) 24 – 151. doi:https://doi.org/10.1016/j.pmatsci.2016.04.001.
URL http://www.sciencedirect.com/science/article/pii/S0079642516300068

[7] N. D. Drummond, V. Zólyomi, V. I. Fal'ko, Electrically tunable band gap in silicene, Phys. Rev. B 85 (2012) 075423. doi:10.1103/PhysRevB.85.075423.
URL https://link.aps.org/doi/10.1103/PhysRevB.85.075423

[8] T.-T. Jia, X.-Y. Fan, M.-M. Zheng, G. Chen, Silicene nanomeshes: bandgap opening by bond symmetry breaking and uniaxial strain, Scientific Reports 6 (1) (2016) 20971. doi:10.1038/srep20971.
URL https://doi.org/10.1038/srep20971

[9] R. Quhe, R. Fei, Q. Liu, J. Zheng, H. Li, C. Xu, Z. Ni, Y. Wang, D. Yu, Z. Gao, J. Lu, Tunable and sizable band gap in silicene by surface adsorption, Scientific Reports 2 (1) (2012) 853. doi:10.1038/srep00853.
URL https://doi.org/10.1038/srep00853

[10] H. Liu, N. Han, J. Zhao, Band gap opening in bilayer silicene by alkali metal intercalation, Journal of Physics: Condensed Matter 26 (47) (2014) 475303. doi:10.1088/0953-8984/26/47/475303.
URL https://doi.org/10.1088%2F0953-8984%2F26%2F47%2F475303

[11] N. Yin, Y. Dai, W. Wei, B. Huang, Electronic structure engineering in silicene via atom substitution and a new two-dimensional dirac structure si3c, Physica E: Low-dimensional Systems and Nanostructures 98 (2018) 39 – 44. doi:https://doi.org/10.1016/j.physe.2017.12.024.

URL http://www.sciencedirect.com/science/article/pii/S1386947717317174

[12] R. E. Roman, S. W. Cranford, Mechanical properties of silicene, Computational Materials Science 82 (2014) 50 – 55. doi:https://doi.org/10.1016/j.commatsci.2013.09.030.
URL http://www.sciencedirect.com/science/article/pii/S092702561300565X

[13] Y. Wang, Y. Ding, Strain-induced self-doping in silicene and germanene from first-principles, Solid State Communications 155 (2013) 6 – 11. doi:https://doi.org/10.1016/j.ssc.2012.10.044.
URL http://www.sciencedirect.com/science/article/pii/S003810981200614X

[14] T. P. Kaloni, Y. C. Cheng, U. Schwingenschlgl, Hole doped dirac states in silicene by biaxial tensile strain, Journal of Applied Physics 113 (10) (2013) 104305. arXiv:https://doi.org/10.1063/1.4794812, doi:10.1063/1.4794812.
URL https://doi.org/10.1063/1.4794812

[15] R. Qin, C.-H. Wang, W. Zhu, Y. Zhang, First-principles calculations of mechanical and electronic properties of silicene under strain, AIP Advances 2 (2) (2012) 022159. arXiv:https://doi.org/10.1063/1.4732134, doi:10.1063/1.4732134.
URL https://doi.org/10.1063/1.4732134

[16] Q. Peng, X. Wen, S. De, Mechanical stabilities of silicene, RSC Adv. 3 (2013) 13772–13781. doi:10.1039/C3RA41347K.
URL http://dx.doi.org/10.1039/C3RA41347K

[17] K. Zberecki, M. Wierzbicki, J. Barnaś, R. Swirkowicz, Thermoelectric effects in silicene nanoribbons, Phys. Rev. B 88 (2013) 115404. doi:10.1103/PhysRevB.88.115404.
URL https://link.aps.org/doi/10.1103/PhysRevB.88.115404

[18] K. Zberecki, R. Swirkowicz, J. Barnaś, Spin effects in thermoelectric properties of al- and p-doped zigzag silicene nanoribbons, Phys. Rev. B 89 (2014) 165419. doi:10.1103/PhysRevB.89.165419.
URL https://link.aps.org/doi/10.1103/PhysRevB.89.165419

[19] N. R. Abdullah, Optical control of spin-dependent thermal transport in a quantum ring, Physics Letters A 382 (21) (2018) 1432–1436. doi:10.1016/j.physleta.2018.03.042.
URL http://www.sciencedirect.com/science/article/pii/S0375960118303177

[20] M. Hu, X. Zhang, D. Poulikakos, Anomalous thermal response of silicene to uniaxial stretching, Phys. Rev. B 87 (2013) 195417. doi:10.1103/PhysRevB.87.195417.
URL https://link.aps.org/doi/10.1103/PhysRevB.87.195417

[21] N. R. Abdullah, T. Arnold, C.-S. Tang, A. Manolescu, V. Gudmundsson, Photon-induced tunability of the thermospin current in a rashba ring, Journal of Physics: Condensed Matter 30 (14) (2018) 145303. doi:10.1088/1361-648x/aab255.
URL https://doi.org/10.1088%2F1361-648x%2Faab255

[22] X. Zhang, H. Xie, M. Hu, H. Bao, S. Yue, G. Qin, G. Su, Thermal conductivity of silicene calculated using an optimized stillinger-weber potential, Phys. Rev. B 89 (2014) 054310. doi:10.1103/PhysRevB.89.054310.
URL https://link.aps.org/doi/10.1103/PhysRevB.89.054310

[23] H. Xie, M. Hu, H. Bao, Thermal conductivity of silicene from first-principles, Applied Physics Letters 104 (13) (2014) 131906. arXiv:https://doi.org/10.1063/1.4870586, doi:10.1063/1.4870586.
URL https://doi.org/10.1063/1.4870586

[24] K. Yang, S. Cahangirov, A. Cantarero, A. Rubio, R. D'Agosta, Thermoelectric properties of atomically thin silicene and germanene nanostructures, Phys. Rev. B 89 (2014) 125403. doi:10.1103/PhysRevB.89.125403.
URL https://link.aps.org/doi/10.1103/PhysRevB.89.125403

[25] H. Sadeghi, S. Sangtarash, C. J. Lambert, Enhanced thermoelectric efficiency of porous silicene nanoribbons, Scientific Reports 5 (1) (2015) 9514. doi:10.1038/srep09514.
URL https://doi.org/10.1038/srep09514

[26] Y. F. Li, G. H. Tang, B. Fu, Hydrogenation: An effective strategy to improve the thermoelectric properties of multilayer silicene, Phys. Rev. B 99 (2019) 235428. doi:10.1103/PhysRevB.99.235428.
URL https://link.aps.org/doi/10.1103/PhysRevB.99.235428

[27] T. Hussain, T. Kaewmaraya, S. Chakraborty, R. Ahuja, Defect and substitution-induced silicene sensor to probe toxic gases, The Journal of Physical Chemistry C 120 (44) (2016) 25256–25262. arXiv:https://doi.org/10.1021/acs.jpcc.6b08973, doi:10.1021/acs.jpcc.6b08973.
URL https://doi.org/10.1021/acs.jpcc.6b08973

[28] A. Molle, C. Grazianetti, L. Tao, D. Taneja, M. H. Alam, D. Akinwande, Silicene, silicene derivatives, and their device applications, Chem. Soc. Rev. 47 (2018) 6370–6387. doi:10.1039/C8CS00338F.
URL http://dx.doi.org/10.1039/C8CS00338F

[29] V. Gudmundsson, H. Gestsson, N. R. Abdullah, C.-S. Tang, A. Manolescu, V. Moldoveanu, Coexisting spin and rabi oscillations at intermediate time regimes in electron transport through a photon cavity, Beilstein Journal of Nanotechnology 10 (1) (2019) 606–616.

[30] K. Chinnathambi, A. Chakrabarti, A. Banerjee, S. Deb, Optical properties of graphene-like two dimensional silicene, arXiv preprint arXiv:1205.5099 (2012).

[31] X.-S. Ye, Z.-G. Shao, H. Zhao, L. Yang, C.-L. Wang, Electronic and optical properties of silicene nanomeshes, RSC Adv. 4 (2014) 37998–38003. doi:10.1039/C4RA03942D.
URL http://dx.doi.org/10.1039/C4RA03942D

[32] C.-H. Wu, Dynamical polarization and the optical response of silicene and related materials, Results in Physics 11 (2018) 665 – 673. doi:https://doi.org/10.1016/j.rinp.2018.10.009.
URL http://www.sciencedirect.com/science/article/pii/S2211379718319132

[33] A. Kokalj, Xcrysden—a new program for displaying crystalline structures and electron densities, Journal of Molecular Graphics and Modelling 17 (3) (1999) 176–179. doi:10.1016/S1093-3263(99)00028-5.
URL http://www.sciencedirect.com/science/article/pii/S1093326399000285

[34] K. Momma, F. Izumi, Vesta 3 for three-dimensional visualization of crystal, volumetric and morphology data, Journal of applied crystallography 44 (6) (2011) 1272–1276.

[35] J. P. Perdew, K. Burke, M. Ernzerhof, Generalized gradient approximation made simple, Phys. Rev. Lett. 77 (1996) 3865–3868. doi:10.1103/PhysRevLett.77.3865.
URL https://link.aps.org/doi/10.1103/PhysRevLett.77.3865

[36] P. Giannozzi, S. Baroni, N. Bonini, M. Calandra, R. Car, C. Cavazzoni, D. Ceresoli, G. L. Chiarotti, M. Cococcioni, I. Dabo, A. D. Corso, S. de Gironcoli, S. Fabris, G. Fratesi, R. Gebauer, U. Gerstmann, C. Gougoussis, A. Kokalj, M. Lazzeri, L. Martin-Samos, N. Marzari, F. Mauri, R. Mazzarello, S. Paolini, A. Pasquarello, L. Paulatto, C. Sbraccia, S. Scandolo, G. Sclauzero, A. P. Seitsonen, A. Smogunov, P. Umari, R. M. Wentzcovitch, QUANTUM ESPRESSO: a modular and open-source software project for quantum simulations of materials, Journal of Physics: Condensed Matter 21 (39) (2009) 395502. doi:10.1088/0953-8984/21/39/395502.
URL https://doi.org/10.1088%2F0953-8984%2F21%2F39%2F395502

[37] P. Giannozzi, O. Andreussi, T. Brumme, O. Bunau, M. B. Nardelli, M. Calandra, R. Car, C. Cavazzoni, D. Ceresoli, M. Cococcioni, et al., Advanced capabilities for materials modelling with quantum espresso, Journal of Physics: Condensed Matter 29 (46) (2017) 465901.

[38] H. J. Monkhorst, J. D. Pack, Special points for brillouin-zone integrations, Phys. Rev. B 13 (1976) 5188–5192. doi:10.1103/PhysRevB.13.5188.

URL https://link.aps.org/doi/10.1103/PhysRevB.13.5188
[39] W. Tang, E. Sanville, G. Henkelman, A grid-based bader analysis algorithm without lattice bias, Journal of Physics: Condensed Matter 21 (8) (2009) 084204. doi:10.1088/0953-8984/21/8/084204.
URL https://doi.org/10.1088%2F0953-8984%2F21%2F8%2F084204
[40] G. K. Madsen, D. J. Singh, Boltztrap. a code for calculating band-structure dependent quantities, Computer Physics Communications 175 (1) (2006) 67–71.
[41] N. R. Abdullah, G. A. Mohammed, H. O. Rashid, V. Gudmundsson, Electronic, thermal, and optical properties of graphene like sicx structures: Significant effects of si atom configurations, Physics Letters A 384 (24) (2020) 126578. doi:https://doi.org/10.1016/j.physleta.2020.126578.
URL http://www.sciencedirect.com/science/article/pii/S037596012030445X
[42] H. O. Rashid, N. R. Abdullah, V. Gudmundsson, Silicon on a graphene nanosheet with triangle- and dot-shape: Electronic structure, specific heat, and thermal conductivity from first-principle calculations, Results in Physics 15 (2019) 102625. doi:10.1016/j.rinp.2019.102625.
URL http://www.sciencedirect.com/science/article/pii/S2211379719317140
[43] N. R. Abdullah, D. A. Abdalla, T. Y. Ahmed, S. W. Abdulqadr, H. O. Rashid, Effect of bn dimers on the stability, electronic, and thermal properties of monolayer graphene, Results in Physics (2020) 103282doi:https://doi.org/10.1016/j.rinp.2020.103282.
URL http://www.sciencedirect.com/science/article/pii/S2211379720317496
[44] S. Cahangirov, M. Topsakal, E. Aktürk, H. Şahin, S. Ciraci, Two- and one-dimensional honeycomb structures of silicon and germanium, Phys. Rev. Lett. 102 (2009) 236804. doi:10.1103/PhysRevLett.102.236804.
URL https://link.aps.org/doi/10.1103/PhysRevLett.102.236804
[45] M. Aliofkhazraei, N. Ali, W. I. Milne, C. S. Ozkan, S. Mitura, J. L. Gervasoni, Graphene Science Handbook: Nanostructure and Atomic Arrangement, CRC Press, 2016.
[46] N. Al-Aqtash, K. M. Al-Tarawneh, T. Tawalbeh, I. Vasiliev, Ab initio study of the interactions between boron and nitrogen dopants in graphene, Journal of Applied Physics 112 (3) (2012) 034304. arXiv:https://doi.org/10.1063/1.4742063, doi:10.1063/1.4742063.
URL https://doi.org/10.1063/1.4742063
[47] N. R. Abdullah, H. O. Rashid, M. T. Kareem, C.-S. Tang, A. Manolescu, V. Gudmundsson, Effects of bonded and non-bonded b/n codoping of graphene on its stability, interaction energy, electronic structure, and power factor, Physics Letters A 384 (12) (2020) 126350. doi:10.1016/j.physleta.2020.126350.
URL http://www.sciencedirect.com/science/article/pii/S0375960120301602
[48] B. Mortazavi, O. Rahaman, M. Makaremi, A. Dianat, G. Cuniberti, T. Rabczuk, First-principles investigation of mechanical properties of silicene, germanene and stanene, Physica E: Low-dimensional Systems and Nanostructures 87 (2017) 228 – 232. doi:https://doi.org/10.1016/j.physe.2016.10.047.
URL http://www.sciencedirect.com/science/article/pii/S1386947716305690
[49] N. R. Abdullah, H. O. Rashid, C.-S. Tang, A. Manolescu, V. Gudmundsson, Modeling electronic, mechanical, optical and thermal properties of graphene-like bc6n materials: Role of prominent bn-bonds, arXiv:2003.08467 [cond-mat.mes-hall] (2020).
URL https://arxiv.org/abs/2003.08467
[50] T. Suzuki, Y. Yokomizo, Silicene: Prediction, synthesis, application, Physica E 40 (2010) 2820.
[51] G. Rahman, Distortion and electric-field control of the band structure of silicene, EPL (Europhysics Letters) 105 (3) (2014) 37012. doi:10.1209/0295-5075/105/37012.
URL https://doi.org/10.1209%2F0295-5075%2F105%2F37012
[52] J. Sivek, H. Sahin, B. Partoens, F. M. Peeters, Adsorption and absorption of boron, nitrogen, aluminum, and phosphorus on silicene: Stability and electronic and phonon properties, Phys. Rev. B 87 (2013) 085444. doi:10.1103/PhysRevB.87.085444.
URL https://link.aps.org/doi/10.1103/PhysRevB.87.085444
[53] N. M. Gabor, J. C. W. Song, Q. Ma, N. L. Nair, T. Taychatanapat, K. Watanabe, T. Taniguchi, L. S. Levitov, P. Jarillo-Herrero, Hot carrier–assisted intrinsic photoresponse in graphene, Science 334 (6056) (2011) 648–652. arXiv:https://science.sciencemag.org/content/334/6056/648.full.pdf, doi:10.1126/science.1211384.
URL https://science.sciencemag.org/content/334/6056/648
[54] S. Das Sarma, E. H. Hwang, Density-dependent electrical conductivity in suspended graphene: Approaching the dirac point in transport, Phys. Rev. B 87 (2013) 035415. doi:10.1103/PhysRevB.87.035415.
URL https://link.aps.org/doi/10.1103/PhysRevB.87.035415
[55] N. R. Abdullah, C.-S. Tang, A. Manolescu, V. Gudmundsson, Effects of photon field on heat transport through a quantum wire attached to leads, Physics Letters A 382 (4) (2018) 199 – 204. doi:https://doi.org/10.1016/j.physleta.2017.11.007.
URL http://www.sciencedirect.com/science/article/pii/S0375960117311209
[56] N. R. Abdullah, C.-S. Tang, A. Manolescu, V. Gudmundsson, Thermoelectric inversion in a resonant quantum dot-cavity system in the steady-state regime, Nanomaterials 9 (5) (2019) 741.
[57] N. R. Abdullah, C.-S. Tang, A. Manolescu, V. Gudmundsson, Manifestation of the purcell effect in current transport through a dotcavityqed system, Nanomaterials 9 (7) (2019) 1023. doi:10.3390/nano9071023.
URL http://dx.doi.org/10.3390/nano9071023
[58] N. R. Abdullah, C.-S. Tang, A. Manolescu, V. Gudmundsson, The photocurrent generated by photon replica states of an off-resonantly coupled dot-cavity system, Scientific Reports 9 (1) (2019) 14703. doi:10.1038/s41598-019-51320-8.
URL https://doi.org/10.1038/s41598-019-51320-8
[59] S. Chowdhury, D. Jana, A theoretical review on electronic, magnetic and optical properties of silicene, Reports on Progress in Physics 79 (12) (2016) 126501. doi:10.1088/0034-4885/79/12/126501.
URL https://doi.org/10.1088%2F0034-4885%2F79%2F12%2F126501
[60] L. L. Yan Voon, G. Guzmn-Verri, Is silicene the next graphene?, MRS Bulletin 39 (4) (2014) 366373. doi:10.1557/mrs.2014.60.
[61] R. John, B. Merlin, Optical properties of graphene, silicene, germanene, and stanene from ir to far uv a first principles study, Journal of Physics and Chemistry of Solids 110 (2017) 307 – 315. doi:https://doi.org/10.1016/j.jpcs.2017.06.026.
URL http://www.sciencedirect.com/science/article/pii/S0022369717300367